cAMP molecule was dependent on the presence of G proteins (Fig. 4B). The effects of GTP occurred when receptors were either phosphorylated or not (Fig. 4B). Thus, it is likely that differences in receptor dissociation kinetics result from altered interactions between the receptors and their coupled G proteins rather than receptor phosphorylation. These data are consistent with previous reports indicating that G proteins influence ligand-binding kinetics of the receptors (*16*).

Previous studies of chemotaxis have shown that signaling events are restricted to the leading edge of the cell (*3*–*6*). The differences in the rates of cAMP binding at the front and back of the cell (Fig. 3) resemble the differences in binding to membranes in the presence and absence of GTP, respectively. The faster cycling at the front may indicate that the G protein complex spends less time in an intermediate state associated with receptor before it is activated by GTP and released. Other studies have suggested that such an intermediate state stabilizes agonist binding (*16*, *24*). The receptors at the leading edge also resemble those in the mutant cells lacking G protein, which seems paradoxical but again may indicate that at the cell anterior, the receptor and G protein spend only a short time in the tight association. Although slightly more G protein is present at the anterior (*7*), the more rapid cycling cannot be simply explained by this difference. A property of the membrane or perhaps a regulator of G protein signaling (RGS) protein may facilitate G protein reactivation at the anterior. It will be important to determine how cells initially form such a polarization in receptor states, whether chemoattractant gradients can modify it, and whether it requires interaction with the cytoskeleton.

References and Notes

1. P. M. W. Janssens, P. J. M. Van Haastert, *Microbiol. Rev.* **51**, 396 (1987).
2. C. A. Parent, P. N. Devreotes, *Annu. Rev. Biochem.* **65**, 411 (1996).
3. ———, *Science* **284**, 765 (1999).
4. Z. Xiao, N. Zhang, D. B. Murphy, P. N. Devreotes, *J. Cell Biol.* **139**, 365 (1997).
5. C. A. Parent, B. Blacklock, W. Froehlich, D. B. Murphy, P. N. Devreotes, *Cell* **95**, 81 (1998).
6. R. Meili *et al.*, *EMBO J.* **18**, 2092 (1999).
7. T. Jin, N. Zhang, Y. Long, C. A. Parent, P. N. Devreotes, *Science* **287**, 1034 (2000).
8. A. Ishijima, T. Yanagida, *Trends Biochem. Sci.* **26**, 438 (2001).
9. M. Tokunaga *et al.*, *Biochem. Biophys. Res. Commun.* **235**, 47 (1997).
10. Y. Sako, S. Minoguchi, T. Yanagida, *Nature Cell Biol.* **2**, 168 (2000).
11. Supplementary Web material (Method of Cy3-cAMP preparation) is available on *Science* Online at www.sciencemag.org/cgi/content/full/294/5543/864/DC1.
12. P. J. M. Van Haastert, E. Kien, *J. Biol. Chem.* **258**, 9636 (1983).
13. T. M. Konijn, P. J. M. Van Haastert, *Methods Cell Biol.* **28**, 283 (1987).
14. P. N. Devreotes *et al.*, *Methods Cell Biol.* **28**, 299 (1987).
15. Chemoattractant-induced F-actin formation was measured as described [A. L. Hall, A. Schlein, J. Condeelis, *J. Cell Biochem.* **37**, 285 (1988)]. The amount of F-actin increased biphasically with two peaks (at 10 s and at 60 to 100 s) by addition of Cy3-cAMP.
16. L. Wu, R. Valkema, P. J. M. Van Haastert, P. N. Devreotes, *J. Cell Biol.* **129**, 1667 (1995).
17. Z. Xiao, Y. Yao, Y. Long, P. N. Devreotes, *J. Biol. Chem.* **274**, 1440 (1999).
18. D. A. Jans, *Biochem. Biophys. Acta* **1113**, 271 (1992).
19. *Dictyostelium discoideum* cells (strain AX2) were cultured axenically with standard culture techniques (*25*). Cells were starved in Sörensen's phosphate buffer (14.6 mM KH_2PO_4, 2 mM Na_2HPO_4, pH 6.0) for 6 hours and then treated with 5 mM caffeine for 30 min to inhibit adenylate cyclase (*14*). After the cells were suspended in the buffer supplemented with 2 mM $MgSO_4$, 5 mM caffeine, and 1 mM dithiothreitol (DTT), an aliquot was placed on a glass cover slip and covered with a thin agarose sheet (*26*). For the chemotactic assay, a small droplet of Cy3-cAMP solution (0.5 to 1 μM) was placed on the agar sheet. The cells in the field of about 1 to 2 mm away from the droplet of Cy3-cAMP were observed.
20. P. J. M. Van Haastert, R. J. W. de Wit, *J. Biol. Chem.* **259**, 13321 (1984).
21. ———, P. M. Janssens, F. Kesbeke, J. DeGoede, *J. Biol. Chem.* **261**, 6904 (1986).
22. The anterior pseudopods or the posterior tails are defined as regions within 10 μm from the leading edge or the rear end of a cell, respectively. The release curves of bound Cy3-cAMP molecules were fitted to the sums of exponentials by the least squares methods with the Levenberg-Marquardt algorithm (KaleidaGraph; Hulinks). The fit was executed for two, three, or four exponentials, because kinetic analysis of cAMP binding to the cells reveals four different forms of its receptors (*1*, *20*, *21*).
23. Membranes were prepared as described (*21*). The wild-type (AX2) and mutant cells in Sörensen's buffer were pretreated for 30 min with either 5 mM caffeine or 10 mM DTT plus 10 μM cAMP to convert the receptors into either the unphosphorylated or phosphorylated states, respectively (*17*). The cells were broken by passing them through a Millipore filter (pore size, 5 μm). After centrifugation of the homogenates, the pellet was collected and resuspended in 10^8 cell equivalents per milliliter in Sörensen's buffer supplemented with 2 mM $MgSO_4$. An aliquot of the suspension was placed on a glass cover slip for 30 min on ice. After washing with the buffer, Cy3-cAMP solution (10 nM) was added. The $G\alpha_2$ null and Gβ null cell lines used in this study are JM1 and LW14, respectively (*16*).
24. A. Levitzki, I. Marbach, A. Bar-Sinai, *Life Sci.* **52**, 2093 (1993).
25. M. Claviez *et al.*, *EMBO J.* **1**, 1017 (1982).
26. S. Yumura, H, Mori, Y. Fukui, *J. Cell Biol.* **99**, 894 (1984).

27. We thank J. West and F. Brozovich for critical reading of the manuscript and our colleagues of the Single-Molecular Processes Project for valuable discussion.

29 June 2001; accepted 31 August 2001

Recruitment of Mec1 and Ddc1 Checkpoint Proteins to Double-Strand Breaks Through Distinct Mechanisms

Tae Kondo,[1]* Tatsushi Wakayama,[1]* Takahiro Naiki,[1]* Kunihiro Matsumoto,[1,2] Katsunori Sugimoto[1]†

In response to DNA damage, eukaryotic cells activate checkpoint pathways that arrest cell cycle progression and induce the expression of genes required for DNA repair. In budding yeast, the homothallic switching (HO) endonuclease creates a site-specific double-strand break at the mating type (*MAT*) locus. Continuous *HO* expression results in the phosphorylation of Rad53, which is dependent on products of the ataxia telangiectasia mutated–related *MEC1* gene and other checkpoint genes, including *DDC1*, *RAD9*, and *RAD24*. Chromatin immunoprecipitation experiments revealed that the Ddc1 protein associates with a region near the *MAT* locus after *HO* expression. Ddc1 association required Rad24 but not Mec1 or Rad9. Mec1 also associated with a region near the cleavage site after *HO* expression, but this association is independent of Ddc1, Rad9, and Rad24. Thus, Mec1 and Ddc1 are recruited independently to sites of DNA damage, suggesting the existence of two separate mechanisms involved in recognition of DNA damage.

When DNA is damaged, cells activate a response pathway that arrests the cell cycle and induces the transcription of genes that facilitate repair. The failure of this response results in genomic instability that may lead to cancer in higher eukaryotes (*1*). The systems that monitor the structure of the chromosomes and coordinate repair and cell-cycle progression are termed "checkpoints" in eukaryotic cells. In budding yeast, two essential genes, *MEC1* and *RAD53*, form the core of the DNA damage checkpoint pathway (*2*, *3*). Mec1 belongs to a superfamily of large protein kinases, including human ATM and ATM-

[1]Division of Biological Science, Graduate School of Science, Nagoya University, [2]CREST, Japan Science and Technology Corporation, Chikusa-ku, Nagoya 464-0814, Japan.

*These authors contributed equally to this work.
†To whom correspondence should be addressed. E-mail: j46036a@nucc.cc.nagoya-u.ac.jp

Rad3-related (ATR). *RAD53* encodes a protein kinase similar to human Chk2 that functions downstream of *MEC1* in the response pathway (*1*, *3*). After DNA damage, Rad53 is phosphorylated and activated by a Mec1-dependent mechanism. Phosphorylation and activation of Rad53 is also dependent on *RAD9* and the genes of the *RAD24* epistasis group, consisting of *DDC1*, *MEC3*, *RAD17*, and *RAD24* (*2*). Homologs of *DDC1*, *MEC3*, *RAD17*, and *RAD24* have been identified in mammalian cells (*1*).

The checkpoint machinery consists of proteins that recognize DNA damage and initiate the signaling response (*1*). Such sensory proteins are expected to bind to the aberrant DNA structures and/or the repair machinery localized on damaged DNA. To address this possibility, we created DNA lesions at a specific sequence and tested whether checkpoint proteins bound to that region. In budding yeast, the HO endonuclease generates a single site-specific double-strand break (DSB) in the genome at the *MAT* locus (*4*). The HO cleavage site is also present at the *HML* and *HMR* loci, but these sites are normally not accessible for cutting. The HO-induced DSB at the *MAT* locus is usually repaired by recombination with the homologous *HML* and *HMR* loci (*4*). When both *HML* and *HMR* are deleted, the HO-induced DSB becomes irreparable by recombination. This persistent DSB is sufficient to cause cells to arrest at the G_2-M phase transition of the cell cycle (*5*–*7*). In the presence of both *HML* and *HMR*, continuous expression of the HO endonuclease results in the persistence of cleaved *MAT* loci and also delays the cell-cycle progression before anaphase (*8*, *9*).

We used an experimental system in which HO endonuclease is continuously expressed to develop an assay for the recruitment of checkpoint proteins. Rad53 is phosphorylated in response to genotoxic stress, and this phosphorylation has been shown to correlate with activation of the DNA damage checkpoint pathway (*2*). We first analyzed the status of Rad53 phosphorylation in cells in which *HO* expression was driven from the galactose-inducible *GAL10* promoter (*10*). Cells expressing the influenza hemagglutinin (HA)–tagged Rad53 (Rad53-HA) protein were transformed with the GAL-HO plasmid or empty vector, and were grown initially in sucrose to repress *HO* expression (*11*). Cells were then transferred to medium containing galactose to induce *HO* expression. Extracts were collected at time intervals and analyzed by Western blot to monitor the modification of Rad53. Rad53 phosphorylation became detectable 4 hours after cells carrying the GAL-HO plasmid were shifted to medium containing galactose (Fig. 1A). DNA blot analysis indicated that cleavage at the *MAT* locus occurred within 2 hours and persisted 6 hours after shifting to the galactose medium (*12*, *13*). The lag of time between DSB formation and Rad53 phosphorylation raises a possibility that the checkpoint activation might result from certain DSB repair events. The HO-induced DSB is usually repaired by the RAD52-dependent homologous recombination pathway or in some cases by Ku-dependent nonhomologous end-joining pathway (*4*). However, Rad53 phosphorylation after *HO* expression was still observed in *rad52*Δ and Ku (*hdf1*Δ) mutants (Fig. 1B). The HO-induced DSB activates the checkpoint pathway only when it cannot be efficiently repaired (*14*). Continuous HO cleavage might induce DNA lesions that could not be repaired efficiently by the recombination and end-joining pathways.

DNA damage-induced Rad53 phosphorylation is dependent on checkpoint genes, including *MEC1*, *DDC1*, *MEC3*, *RAD9*, *RAD17*, and *RAD24* (*2*). We examined Rad53 phosphorylation status after *HO* expression in *ddc1*Δ, *mec3*Δ, *rad9*Δ, *rad17*Δ, and *rad24*Δ mutants carrying the GAL-HO and RAD53-HA plasmids. Rad53 phosphorylation after *HO* expression was decreased in *ddc1*Δ, *mec3*Δ, *rad9*Δ, *rad17*Δ, and *rad24*Δ mutants compared with that observed in wild-type cells (Fig. 1C). The *sml1*Δ mutation suppresses the lethality but not the checkpoint defect associated with the *mec1*Δ mutation (*15*). As found in wild-type cells, Rad53 became phosphorylated after *HO* expression in *sml1*Δ cells. In contrast, no Rad53 modification was observed in *mec1*Δ *sml1*Δ mutants (Fig. 1C). Thus, continuous *HO* expression induces phosphorylation of Rad53 in a manner dependent on the *DDC1*, *MEC1*, *MEC3*, *RAD9*, *RAD17*, and *RAD24* genes.

We used an *HO* expression system to examine the recruitment of checkpoint proteins to a region near the HO-cleavage site. Ddc1 forms a complex with Rad17 and Mec3, and this Ddc1-Mec3-Rad17 complex has been suggested to function downstream of Rad24 in the checkpoint pathway (*16*). We examined the association of Ddc1 with sites near the HO-induced DSB with the use of a chromatin immunoprecipitation assay (*17*). Cells expressing the Ddc1-HA protein were transformed with the GAL-HO plasmid or empty vector (*11*). After transformants were grown in sucrose, one-half of the culture was maintained in sucrose and the other half was incubated with galactose for 4 hours to induce *HO* expression. Extracts prepared after formaldehyde cross-linking were subjected to immunoprecipitation with antibody to HA (anti-HA). Precipitated DNAs were extracted and amplified by polymerase chain reaction (PCR) using either primer sets (HO1 and HO2) corresponding to regions near the HO-restriction site on the *MAT*α locus on chromosome III (Fig. 2A) or primers for the *SMC2* locus containing no cleavage site on chromosome VI. Interaction of Ddc1 with the *MAT*α locus was detected in cells carrying the GAL-HO plasmid after incubation with galactose but not in similarly treated cells carrying the control vector (Fig. 2B). This Ddc1 interaction is specific to the *MAT*α locus because the PCR amplified from the *SMC2* locus did not increase after incubation with galactose (Fig. 2B). Moreover, increase in PCR amplification of the *HML* or *HMR* locus was not detected (*12*), consistent with the observation that the HO endonuclease does not normally generate a DSB at the *HML* or *HMR* locus. The Ddc1 interaction was observed 4 hours after cells were exposed to galactose with a similar kinetics to Rad53 phosphorylation, suggesting a temporal correlation between the Ddc1 interaction and checkpoint activation (Figs. 1A and 2B). PCRs with the primer pairs HO1 and HO2 amplified regions 2.0 and 1.0 kb away from the cleavage site, respectively (Fig. 2A), and Ddc1 interacted with these regions in a similar manner (Fig. 2B). These results suggest that Ddc1 is recruited to sites near the HO-induced DSB.

We next examined whether *RAD9*, *RAD17*, *RAD24*, or *MEC1* is required for the recruitment of Ddc1 to the HO-induced DSB lesions. After *HO* expression, association of Ddc1 with the *MAT*α locus was detected in *rad9*Δ mutants (Fig. 2C). Similarly, that as-

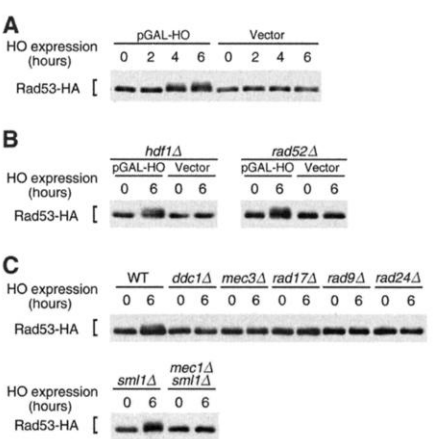

Fig. 1. Rad53 phosphorylation after *HO* expression. (**A**) Wild-type cells containing YCpT-RAD53-HA (*11*) were transformed with pGAL-HO (*10*) or the YCp50 vector. Transformants were grown in sucrose medium without uracil and tryptophan, and transferred to medium containing 2% galactose. At the indicated time points, portions of the cells were harvested for Western blotting analysis (*16*). (**B**) Effect of the *hdf1*Δ and *rad52*Δ mutations on the HO-induced Rad53 phosphorylation. Cells containing YCpT-RAD53-HA and pGAL-HO or the vector were analyzed as in (A). (**C**) Effect of the *ddc1*Δ, *mec3*Δ, *rad17*Δ, *rad9*Δ, *rad24*Δ, and *mec1*Δ mutations on the HO-induced Rad53 phosphorylation. Cells containing YCpT-RAD53-HA and pGAL-HO were analyzed as in (A).

sociation was detected in *mec1Δ sml1Δ* as well as *sml1Δ* strains (Fig. 2C). However, interaction of Ddc1 with the *MATα* locus was not observed in *rad17Δ* or *rad24Δ* mutants (Fig. 2C). These results indicate that the association of Ddc1 with a region near the HO-cleavage site is dependent on *RAD17* and *RAD24* but not on *RAD9* or *MEC1*. One reason that Ddc1 association with the *MATα* locus was not detected in *rad17Δ* and *rad24Δ* mutants could be that these mutations affect nuclear localization of the Ddc1 protein, thereby preventing association with the HO-induced DSB lesions. To address this possibility, we examined Ddc1 localization by immunofluorescence microscopic analysis (Fig. 3) (*18*). Control experiments with wild-type cells expressing untagged Ddc1 revealed no staining. In wild-type cells expressing Ddc1-HA, the tagged Ddc1 proteins were found to localize in the nucleus. Ddc1 localization was unaffected in *rad24Δ* mutants, but in *rad17Δ* mutants the immunofluorescence signal of Ddc1-HA was decreased in the nucleus and distributed diffusely in the cytoplasm. Expression of Ddc1-HA is similar in *rad17Δ* mutants and wild-type cells (*16*, *19*). Because Ddc1 fails to form a complex with Mec3 in *rad17Δ* mutant cells (*16*, *19*), it appears that the assembly of Ddc1 into the Ddc1-Mec3-Rad17 complex may be required for its nuclear localization. If so, the defect in the Ddc1 association with the *MATα* locus in *rad17Δ* mutants may result from the decreased accumulation of Ddc1 in nucleus. In contrast to the *rad17Δ* mutation, the *rad24Δ* mutation does not affect the interaction among Rad17, Mec3, and Ddc1 (*12*, *19*). Together, these results are consistent with a model in which Rad24 regulates the recruitment of the Ddc1-Mec3-Rad17 complex to the HO-induced DSB. In agreement with this model, Mec3 and Rad17 also associate with the *MATα* locus after *HO* expression in a *RAD24* dependent manner (Fig. 4).

Mec1 has a central role in the DNA damage response and has been suggested to function downstream of the Ddc1-Mec3-Rad17 complex. Therefore, we examined the interaction of Mec1 with the HO-induced DSB lesions in cells expressing Mec1-HA and carrying the GAL-HO plasmid or empty vector (*11*). Mec1 association with the *MATα* locus was detected only in cells expressing *HO*, and no association with the *SMC2*, *HML*, or *HMR* loci was detected (Fig. 5) (*12*). The Mec1 association with the *MATα* locus became detectable 4 hours after *HO* expression, as did the Ddc1 interaction (Figs. 2B and 5A). However, the Mec1 association was not dependent on either *RAD9* or *RAD24* (Fig. 5B). Consistent with the observation that *DDC1* functions in the same checkpoint pathway as *RAD24*, the *ddc1Δ* mutation did not affect the Mec1 association (Fig. 5B). Our results suggest that Mec1 and Ddc1 are recruited to sites near the HO-induced DSB through distinct mechanisms.

Rad24 interacts with the small subunits of the replication factor C (RFC) complex (Rfc2, Rfc3, Rfc4, and Rfc5) and forms a complex related to the RFC complex (*20*–*22*). Ddc1, Mec3, and Rad17 are structurally related to the proliferating cell nuclear antigen (PCNA), which forms a doughnut-like homotrimer (*23*–*25*). During DNA replication, the RFC complex binds to PCNA and loads itonto primed DNA (*26*). Given these structural similarities, our results indicate that the Rad24 complex may recognize DNA damage and recruit the Ddc1-Mec3-Rad17 complex to such sites. Ddc1 is phosphorylated after DNA damage in a manner dependent on *RAD24* and *MEC1* (*19*). Because Mec1 is also recruited to DSB lesions, phosphorylation of Ddc1 may be the result from its localization with Mec1 on damaged DNA. What regulates

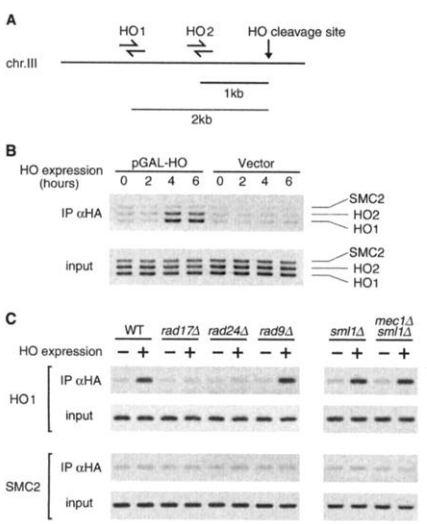

Fig. 2. Association of Ddc1 with sites near the HO-induced DSB. (**A**) The *MATα* locus on chromosome III (chr. III) contains a single HO endonuclease cleavage site. When the HO endonuclease is expressed, it can readily introduce a DSB at the cleavage site. The primer pairs HO1 and HO2 were designed to amplify regions near the cleavage site on the *MATα* locus by PCR. (**B**) Strains (*MATα*, *DDC1-HA*) (*11*) were transformed with pGAL-HO or the YCp50 vector. The resulting strains were grown in sucrose medium without uracil and were transferred to galactose to induce *HO* expression or maintained in sucrose to repress *HO* expression. Cells were then collected at the indicated times for a chromatin immunoprecipitation (IP) assay (*17*). PCR was done with the primers for the *MATα* locus shown schematically in (A) and for the control *SMC2* locus. PCR products from the respective extracts (input) are shown in parallel. (**C**) Effect of the *rad17Δ*, *rad24Δ*, *rad9Δ*, and *mec1Δ* mutations on Ddc1 association with DSB. Cells transformed with pGAL-HO were grown in sucrose medium without uracil and were transferred to galactose to induce *HO* expression (+) or maintained in sucrose to repress *HO* expression (−) for 4 hours. Extracts were prepared from cells and subjected to chromatin immunoprecipitation assay as in (B). Strains used (*11*) contain *MATα* and *DDC1-HA*.

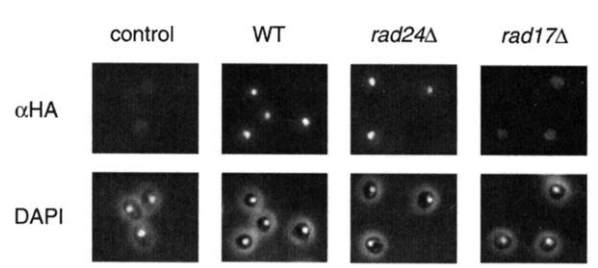

Fig. 3. Intracelluar localization of Ddc1. Cells were grown to mid-log phase and were subjected to immunofluorescence microscopic analysis (*18*). Ddc1 and nucleus were visualized using anti-HA antibody and DAPI (4′,6′-diamidino-2-phenylindole), respectively. Strains used (*11*) are control (*MATα*, *DDC1*), wild-type (*MATα*, *DDC1-HA*), *rad17Δ* (*MATα*, *DDC1-HA*, *rad17Δ*), *rad24Δ* (*MATα*, *DDC1-HA*, *rad24Δ*).

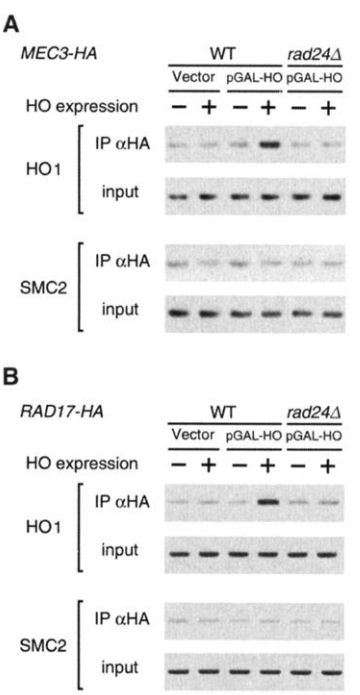

Fig. 4. Association of Mec3 and Rad17 with sites near the HO-induced DSB. Cells transformed with pGAL-HO or the control vector were processed and subjected to a chromatin immunoprecipitation assay, as in Fig. 2C. Strains used (*11*) contain *MATα* and *MEC3-HA* (**A**) or *MATα* and *RAD17-HA* (**B**).

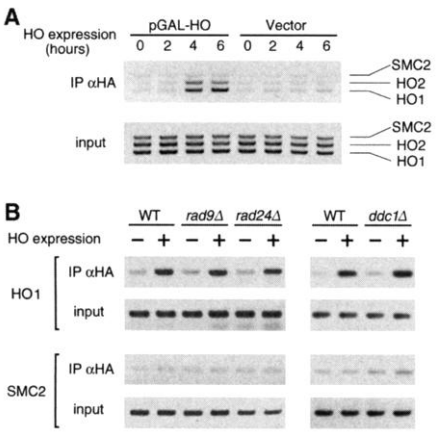

Fig. 5. Association of Mec1 with sites near the HO-induced DSB. (**A**) Kinetics of Mec1 association with DSB. (**B**) Effect of the *rad9Δ*, *rad24Δ*, and *ddc1Δ* mutations on Mec1 association with DSB. Cells transformed with pGAL-HO or the control vector were processed and subjected to a chromatin immunoprecipitation assay, as in Fig. 2B (A) and Fig. 2C (B). Strains used (*11*) contain *MATα* and *MEC1-HA*.

the association of Mec1 with DNA lesions remains to be determined. ATR and hRad9 are human homologs of Mec1 and Ddc1, respectively (*1*), and localize to nuclear foci that may contain regions of damaged DNA (*27*, *28*). Because homologs of the checkpoint genes have been identified in other species, it is likely that the mechanism described here is conserved in the checkpoint control among eukaryotic cells.

References and Notes

1. B.-B. S. Zhou, S. J. Elledge, *Nature* **408**, 433 (2000).
2. M. P. Longhese, M. Foiani, M. Muzi-Falconi, G. Lucchini, P. Plevani, *EMBO J.* **17**, 5525 (1998).
3. S. J. Elledge, *Science* **274**, 1664 (1996).
4. J. E. Haber, *Mutat. Res.* **451**, 53 (2000).
5. L. L. Sandell, V. A. Zakian, *Cell* **75**, 729 (1993).
6. D. P. Toczyski, D. J. Galgoczy, L. H. Hartwell, *Cell* **90**, 1097 (1997).
7. S. E. Lee *et al.*, *Cell* **94**, 399 (1998).
8. L. K. Lewis, J. M. Kirchner, M. A. Resnick, *Mol. Cell. Biol.* **18**, 1891 (1998).
9. J. Demeter, S. E. Lee, J. E. Haber, T. Stearns, *Mol. Cell* **6**, 487 (2000).
10. I. Herskowitz, R. E. Jensen, *Methods Enzymol.* **194**, 132 (1991).
11. All strains were isogenic with KSC006 and were derived using standard genetic techniques. Strains are *MATa* except for those indicated as *MATα*. To express Rad53-HA, cells were transformed with YCpT-RAD53-HA, a *TRP1* marker version of YCpRAD53-HA (*16*).
12. T. Kondo, T. Wakayama, T. Naiki, K. Matsumoto, K. Sugimoto, unpublished data.
13. B. Connolly, C. I. White, J. E. Haber, *Mol. Cell. Biol.* **8**, 2342 (1988).
14. A. Pellicioli, S. E. Lee, C. Lucca, M. Foiani, J. E. Haber, *Mol. Cell* **7**, 293 (2001).
15. X. Zhao, E. G. D. Muller, R. Rothstein, *Mol. Cell* **2**, 329 (1998).
16. T. Kondo, K. Matsumoto, K. Sugimoto, *Mol. Cell. Biol.* **19**, 1136 (1999).
17. Yeast cells were cultured in medium containing 2% sucrose, and then one-half of the culture was maintained in sucrose and the other half was incubated with 2% galactose to induce *HO* expression. Cells were converted to spheroplasts with the use of oxalyticase (50 μg/ml) in 50 mM Hepes-KOH (pH 7.5); 100 mM NaCl; 0.4 M sorbitol; 50 mM NaF; 5 mM PNPP; 1 mM Na3VO4; 0.5 mM PMSF; aprotinin (13 μg/ml); leupeptin (5 μg/ml); pepstatin (5 μg/ml); and 1 mM benzamidine. Spheroplasts were lysed by adding Triton X-100 (0.25%) and were subsequently cross-linked with 1% formaldehyde for 15 min at 4°C. Immunoprecipitation of cross-linked DNA was performed essentially as described (*29*) with the use of monoclonal antibody 12CA5 to HA. DNA was also purified from the whole cell extract (designated "input"). PCR was done in 50-μl volumes containing 1/25 of the anti-HA antibody immunoprecipitates or 1/1200 of input, respectively. The PCR products were separated in 2% agarose gels and were stained with ethidium bromide. The sequences of primers for the are as follows: HO1 set at *MATα* locus, 5′-CCAGATTTGTATTAGACGAGGGACGGAGTGA-3′ and 5′-AGAGGGTCACAGCACTAATACAGCTCGTAAT-3′; HO2 set at *MATα* locus, 5′-GGTGTCCTCTGTAAGGTTTAGTACTTTTGT-3′ and 5′-CACAGATGAGTTTAAATCCAGCATACTAGACA-3′; and *SMC2* locus 5′-AAGAGAAACTTTAGTCAAAACATGGG-3′ and 5′-CCATCACATTATACTAACTACGG-3′.
18. Cells were processed and incubated with mouse antibody to HA (16B12; Babco, Richmond, CA). Antibody binding was detected using Cy3-conjugated anti-mouse antibody (Jackson ImmunoResearch, West Grove, PA).
19. V. Paciotti, G. Lucchini, P. Plevani, M. P. Longhese, *EMBO J.* **17**, 4199 (1998).
20. T. Shimomura, S. Ando, K. Matsumoto, K. Sugimoto, *Mol. Cell. Biol.* **18**, 5485 (1998).
21. C. M. Green, H. Erdjument-Bromage, P. Tempst, N. F. Lowndes, *Curr. Biol.* **10**, 39 (2000).
22. T. Naiki, T. Shimomura, T. Kondo, K. Matsumoto, K. Sugimoto, *Mol. Cell. Biol.* **20**, 5888 (2000).
23. L. Aravind, D. R. Walker, E. V. Koonin, *Nucleic Acids Res.* **27**, 1223 (1999).
24. M. P. Thelen, C. Venclovas, K. Fidelis, *Cell* **96**, 769 (1999).
25. C. Venclovas, M. P. Thelen, *Nucleic Acids Res.* **28**, 2481 (2000).
26. S. Waga, B. Stillman, *Annu. Rev. Biochem.* **67**, 721 (1998).
27. M. A. Burtelow *et al.*, *J. Biol. Chem.* **275**, 26343 (2000).
28. R. S. Tibbetts *et al.*, *Genes Dev.* **14**, 2989 (2000).
29. T. Tanaka, D. Knapp, K. Nasmyth, *Cell* **90**, 649 (1997).

30. We thank M. P. Longhese, G. Lucchini, and T. Weinert for materials; we also thank J. Haber, H. Araki, M. Lamphier, N. F. Lowndes, and H. Masumoto for critical reading, discussion, and suggestion. Supported by grants from the Ministry of Education, Science, Sports and Culture of Japan.

26 June 2001; accepted 20 August 2001

The Plasticity of Dendritic Cell Responses to Pathogens and Their Components

Qian Huang,[1] Dongyu Liu,[1] Paul Majewski,[1] Leah C. Schulte,[1] Joshua M. Korn,[2] Richard A. Young,[1,2] Eric S. Lander,[1,2,3] Nir Hacohen[1]*

Dendritic cells are involved in the initiation of both innate and adaptive immunity. To systematically explore how dendritic cells modulate the immune system in response to different pathogens, we used oligonucleotide microarrays to measure gene expression profiles of dendritic cells in response to *Escherichia coli*, *Candida albicans*, and influenza virus as well as to their molecular components. Both a shared core response and pathogen-specific programs of gene expression were observed upon exposure to each of these pathogens. These results reveal that dendritic cells sense diverse pathogens and elicit tailored pathogen-specific immune responses.

How organisms respond appropriately to the wide variety of pathogens and antigens they encounter on a daily basis remains a central question in immunology. It has recently been shown that pattern recognition receptors expressed on immune cells contribute to the specific detection of pathogens (*1*, *2*). However, the downstream target genes induced by the different pathogens have not been fully determined. The importance of dendritic cells (DCs) in initiating immune responses led us to investigate at a genetic level how DCs discriminate different pathogens (*3*). DCs reside in an immature state in most tissues, where they recognize and phagocytose pathogens and other antigens (*4*). Direct contact with many pathogens leads to the maturation of DCs, which is characterized by an increase in antigen presentation, expression of costimulatory molecules, and subsequent stimulation of naïve T cells in lymphoid organs (*4*). The extensive reprogramming of DCs during maturation prompted us to measure the corresponding changes in gene expression. We used oligonucleotide microarrays (*5*) to test to what extent DCs discriminate between phylogenetically diverse pathogens and whether the commonly studied molecular components of these pathogens are sufficient to account for the live pathogen response.

Human monocyte-derived DCs (*6*) were exposed to a diverse set of organisms and com-

[1]Whitehead Institute for Biomedical Research, Cambridge, MA 02142, USA. [2]Department of Biology, Massachusetts Institute of Technology, Cambridge, MA 02142, USA. [3]Whitehead Institute Center for Genome Research, Cambridge, MA 02139, USA.

*To whom correspondence should be addressed. E-mail: hacohen@wi.mit.edu